

Multi-Center Hyperbonding in Phase-Change Materials

Tae Hoon Lee* and Stephen R. Elliott*

A comprehensive understanding of chemical interactions underlying the network structure of chalcogenide materials is a crucial prerequisite for comprehending their microscopic structures, physicochemical properties, and capabilities for current or potential applications. However, for many chalcogenide materials, an inherent difficulty is often present in investigating their chemical properties, due to the involvement of delocalized bonding and non-bonding (“lone-pair”) electrons, which requires interaction mechanisms beyond that of conventional two-center, two-electron covalent bonding. Herein, some recent progress in the development of new interatomic interaction models for chalcogenides is reviewed, in particular focusing on the multi-center hyperbonding model, proposed in an effort to resolve this issue. The capability of this model in elucidating a diversity of interesting material properties of phase-change materials (PCMs) is highlighted, including Ge₂Sb₂Te₅ (GST). These include the propensity of high coordination numbers of constituent atoms, linear triatomic bonding geometries with short and long bonds (often ascribed to the effect of a Peierls distortion), abnormally large Born effective charges of crystalline GST, large optical contrast between amorphous and crystalline GST, ultrafast crystallization speed of amorphous GST, and the chemical origin differentiating non-PCM from PCM chalcogenide materials. Other bonding models for these materials are also briefly discussed.

recently with the advent of density-functional theory (DFT)-based ab initio methods, capable of simulating reasonably large model systems of more than a few hundred atoms.^[2,3] The recent development of the first-principles DFT calculations has, hence, brought about a significant reform of the research on chalcogenides by providing an accurate tool for analyzing and predicting chalcogenide properties, thereby paving the way for in silico materials discovery. Combined with experimental methods, a wide range of chalcogenide compositions are now routinely investigated computationally in diverse research areas, including topological insulators,^[4] memory devices,^[5] thermoelectric energy conversion,^[6] etc.

Phase-change (memory) materials (PCMs), a subgroup of chalcogenide materials, have been of great scientific and industrial interest due to their unique material properties, leading to the next-generation of optical/electronic memory technology.^[5,7] The majority of PCMs reported so far are telluride compounds.^[8]


This is because, in most cases, the prerequisite material conditions for the non-volatile memory application are met only by this material type. On the other hand, most sulfide or selenide compounds seldom fulfil the required conditions, for instance, for a large optical contrast between their amorphous (*a*-) and crystalline (*c*-) phases, and of an ultrafast crystallization speed of the *a*-phase, on the order of tens to hundreds of nanoseconds. The former requirement of a large optical contrast corresponds to there being a large difference in dielectric constants or Born effective charges (BECs) between the two phases, whereas the latter fast crystallization is associated with facile local structural changes or valence-charge redistribution in amorphous PCMs.^[9] From a structural point of view, these two material requirements appear to be in conflict with each other, in that large (small) overall structural changes are anticipated for the former (latter) condition, respectively. More recently, it has also been reported^[10] that PCMs are good candidate materials for thermoelectric energy conversion, exhibiting high thermoelectric figures of merit. Their small values of lattice thermal conductivities were attributed to the presence of large anharmonicity.^[11,12] Zeier et al.^[13] also revealed rather general correlations between small values of the lattice thermal conductivity and chemical-bonding properties of the constituent elements, such as a large coordination number or long bond lengths.

Here, we attempt to address the question of how to understand the interesting material properties of chalcogenide PCMs, and of some non-PCMs, from the point of view of the multi-center

1. Introduction

Amorphous chalcogenide materials, containing heavy tellurium atoms, tend to exhibit complicated interatomic interactions, which are often challenging to be thoroughly analyzed experimentally.^[1] This circumstance has been dramatically changed

Dr. T. H. Lee,^[+] Prof. S. R. Elliott,^{[++],[+++]}
Department of Chemistry
University of Cambridge
Lensfield Road, Cambridge CB2 1EW, UK
E-mail: th132@cam.ac.uk, sre1@cam.ac.uk

 The ORCID identification number(s) for the author(s) of this article can be found under <https://doi.org/10.1002/pssr.202000516>.

^[+]Present address: Department of Engineering, University of Cambridge, Cambridge CB3 0FA, UK

^[++]Present address: Trinity College, University of Cambridge, Cambridge CB2 1TQ, UK

^[+++]Present address: Department of Chemistry, University of Oxford, Oxford OX1 3TF, UK

© 2021 The Authors. Physica Status Solidi (RRL) – Rapid Research Letters published by Wiley-VCH GmbH. This is an open access article under the terms of the Creative Commons Attribution License, which permits use, distribution and reproduction in any medium, provided the original work is properly cited.

DOI: 10.1002/pssr.202000516

hyperbonding model developed recently through the first-principles DFT simulations.^[14] Although we focus here on the $\text{Ge}_2\text{Sb}_2\text{Te}_5$ (GST) material, the prototypical PCM, the conclusions are quite general for other PCMs and non-PCM chalcogenides.

2. Requirement for a New Bonding Concept Beyond the Lewis Two-Center, Two-Electron Model

The conventional description of chemical interactions for main-group semiconductor materials involves two-center, two-electron (2c/2e) (polar) covalent bonds.^[15] This is most obvious for monoatomic materials of tetrahedrally coordinated atoms, such as group-IV (e.g., Si or Ge) semiconductors, or chalcogenides consisting of tetrahedral cations and divalent chalcogen anions, such as group IV–VI₂ (e.g., GeS_2) semiconductors, with sp^3 hybridized atomic orbitals (AOs) being involved in bonding, and satisfying the Lewis octet rule. However, the situation becomes more complicated for non-tetrahedrally bonded compounds, as lone pairs (LPs), in particular, of chalcogen atoms tend to interact with neighboring unoccupied antibonding orbitals. This extra interaction, which is different from the ordinary 2c/2e bond, often gives rise to local violations of the octet rule.

To clarify the limitation of describing chemical interactions in PCMs solely with ordinary 2c/2e covalent bonds and the octet rule, we consider two hypothetical cases, in which: 1) the interatomic interactions in *a*-GST are fully describable solely with 2c/2e covalent bonds and the Lewis octet rule is strictly obeyed; and 2) additional types of interatomic interactions coexist with the 2c/2e covalent bonding mechanism, and a violation of the octet rule is allowed. Let us first assume that the former case 1) is fully satisfied; i.e., the valence-charge distribution is accurately approximated by localized non-bonding and 2c/2e bonding valence-electron pairs. In this case, the total number of electron

pairs, and AOs, involved in bonding and non-bonding for each atom is four; therefore, eight electrons are associated with each atom, satisfying the Lewis octet rule. With this hypothesis, the electron configuration of Sb (s^2p^3) in *a*-GST would lead to a pyramidal local coordination geometry, with each apex occupied by three ligand Te atoms (each forming a covalent bond with the central Sb atom) and a single LP on the central Sb atom (see Figure 1). Following Lee and Elliott,^[9] this configuration can be denoted, for simplicity, as Sb(3,1), where the former and latter numbers in parentheses indicate the number of associated bonds and of LPs, respectively, for the central atom. The same local structure of Ge(3,1) also conforms to the octet rule, but not strictly to the 8-*N* rule, as four bonds are dictated by the latter rule. Tetrahedral Ge(4,0) units satisfy both rules. In *a*-GST, the (3,1) coordination type turns out to constitute the majority of molecular structural motifs for Sb and Ge atoms. Similarly, the dominant structural units for Te atoms are Te(2,2) and Te(3,1), both of which satisfy the Lewis octet rule. Figure 1 summarizes the main structural units, with assigned numbers of bonds and of LPs observed in *a*-GST. The majority of individual structural units indeed satisfy the octet rule by possessing, in total, four pairs of covalent bonds and LPs. However, there also exist a non-negligible percentage (11% in *a*-GST) of structural units whose associated number of bonds and LPs exceeds four, requiring more than four AOs to be involved in bonding. The hypothesis of perfect Lewis-type local coordination in *a*-GST is, hence, a poor approximation in describing actually calculated charge distributions; that is, the Lewis picture alone is incomplete for describing the chemical interactions in *a*-GST (and other PCMs), and the second scenario (2), involving the presence of additional types of interactions, should be adopted instead.

It should be noted that, in extracting the number of chemical bonds and LPs from DFT calculations, the maximally localized Wannier function (MLWF)^[16] representation was used. In this case, the electron-charge distributions obtained from delocalized

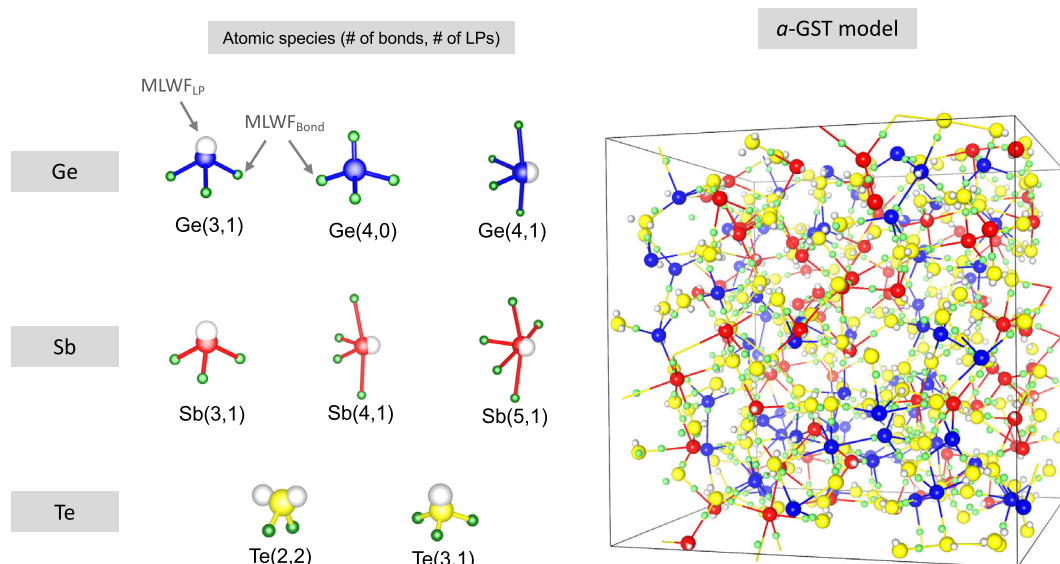


Figure 1. Amorphous GST model and constituent structural units. The numbers in parentheses from left to right indicate the number of bonds and LPs associated with the central atom, respectively. Adjacent structural units share a bond MLWF ($\text{MLWF}_{\text{bond}}$). The whole amorphous network (right) can then be constructed from the interconnected structural units (left).

Kohn–Sham (KS) orbitals were represented in terms of localized Wannier functions by unitary transformations, each of which is considered here as representing either a bond or LP, depending on the criteria for bond formation defined in the analysis.^[9,17]

3. Multi-Center Hyperbonding

3.1. Rise of a Hyperbonding Concept

The need for revising the $2c/2e$ covalent-bond-only picture for describing a -GST arises due to the significant delocalization of valence electrons that are involved in beyond-two-body interactions. The task is then how to link the propensity of valence-electron delocalization to the structural units that do not satisfy the octet rule in a -GST. To do so, the nature of chemical bonding in a -GST should be investigated in more detail. A hint on this was provided by Kolobov et al.,^[18] and a more comprehensive description has been proposed by Lee and Elliott.^[14] Unlike the structural units satisfying the octet rule, such as (3,1) or (2,2) types, structural units, which are incompatible with the Lewis picture, commonly possess at least a single linear triatomic bonding motif (**Figure 2**), and, for each triatomic bonding motif, three atoms form two joined bonds with a bond angle of $\approx 180^\circ$. For such structural units, this (near-) linear triatomic configuration does not fit into the conventional two-body description based on sp -hybridized AOs, as more than four AOs are required for the main-group Ge and Sb atoms. Correspondingly, the properties of the two linked bonds constituting the linear triatomic motif are chemically distinct from those of ordinary $2c/2e$ covalent bonds. For instance, compared with $2c/2e$ covalent bonds, the two bonds constituting a linear triatomic motif of a “seesaw” Sb(4,1) unit display a longer bond length, weaker bond strength, stronger polarity, and higher delocalization of electrons involved in bonding (**Figure 2**).^[9] The same trend is also observed for the square pyramidal Sb(5,1) units.

Interestingly, the denoted property contrast between the linear triatomic bonds and ordinary covalent bonds of (4,1)-type units in a -GST closely corresponds to the property difference between the respective axial and equatorial bonds in hypervalent molecules with a similar molecular geometry.^[19] Here, hypervalent molecules refer to the molecular species, any of whose constituent main-group elements have, in total, more than four associated bonding and non-bonding electron pairs.^[19,20] This means that they violate the octet rule, as do the central atoms of structural units that have linear triatomic bonds in a -GST. It is this similarity in structure and properties that rationalizes the description of the linear triatomic bonds in a -GST in terms of the concept of “hyperbonds,” which has been successfully adopted to describe linear triatomic bonds in molecules.^[21] The term “hyperbond” is coined here to denote one of the two connected bonds constituting a (near-) linear triatomic bonding motif with shared similar chemical properties; hence, the term hyperbond pair is alternatively used to indicate a linear triatomic bonding geometry. This hyperbonding concept plays a significant role in understanding the chemical-bonding interactions in a -GST, and other chalcogenides in general. The (4,1)-type unit with the seesaw local-bonding geometry has a single linear triatomic bonding geometry (i.e., two hyperbonds) and two ordinary $2c/2e$ bonds. On the other hand, the (5,1)-type unit, with a square-pyramidal bonding configuration, consists of two perpendicular hyperbond pairs (i.e., four hyperbonds) and a single ordinary covalent bond (**Figure 2**). It should be noted that the overall distributions of bonding and non-bonding electron pairs for all the structural units shown in **Figure 1** and **2** conform to the molecular geometry predicted by the valence-shell electron-pair repulsion (VSEPR) theory.^[22]

3.2. Theoretical Background of the Hyperbonding Model

The bonding concept for the linear triatomic bonding motif was initially elucidated by three-center, four-electron ($3c/4e$) bonding

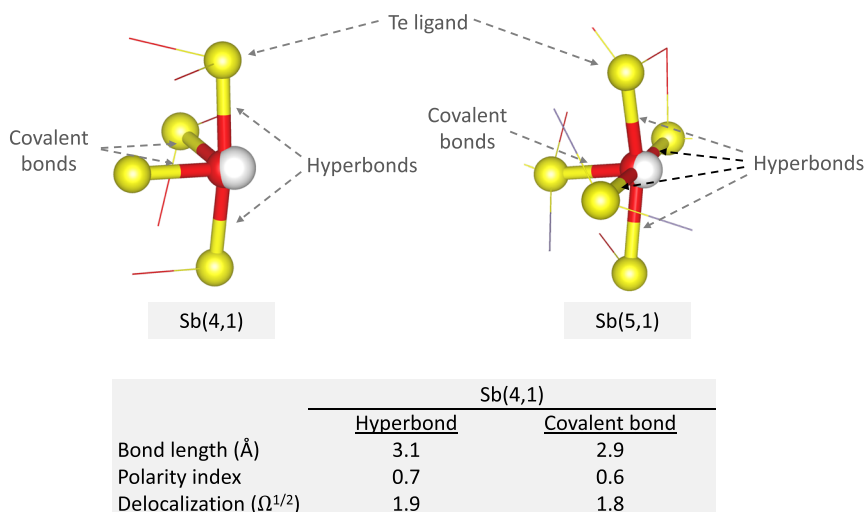


Figure 2. Representative Sb-centered structural units with the number of bonds and LPs exceeding four. These two units violate the octet rule. A comparison of bonding characteristics between the hyperbonds and covalent bonds for a Sb(4,1) unit (denoted in the figure) is shown in the table. The values are averaged over all the units of the same type in the a -GST model. The definition of polarity index corresponds to the value of χ described in the previous study.^[14]

in a molecular-orbital (MO) picture^[23] in an effort to understand the formation of halogen molecules with linear triatomic bonding geometries. Non-zero bond orders arise from the filled bonding and nonbonding MOs constructed from the relevant three valence AOs. The valence-bond perspective of this 3c/4e MO description has been recently complemented by the charge-shift bonding model, which includes the effect due to mixing of covalent and ionic structures.^[24]

On the other hand, the hyperbonding concept, which is eventually equivalent to the 3c/4e MO description,^[25] is based on the natural bond-orbital (NBO) perspective with a donor–acceptor paradigm.^[21] We discuss the underlying principles of hyperbonding by considering again the case of *a*-GST. An LP of a Te (A) atom (whose state is denoted as n_A) tends to be delocalized to a nearby unoccupied antibonding state (σ_{BC}^*) of a pair of bonded, say, Sb (B) and Te (C), atoms (Figure 3a). As the interaction between the Te LP and the nearby antibonding orbital σ_{BC}^* is allowed, the Lewis 2c/2e bonding picture is no longer complete (Figure 3a-i), and delocalization-induced interactions should be considered additionally. Figure 3a-ii,iii corresponds to this case, in which multi-center interactions are now allowed, and the initial 2c/2e covalent bonds are strongly affected by this perturbation accordingly. The resultant stabilization interaction of the n_A state leads to a lowering of its energy (Figure 3b). At the same time, the overall bond order for the original B and C atom pair is reduced with the occupation of its antibonding state. As three atoms (A, B, and C) with four valence electrons are involved in this interaction, it is referred to as a three-center, four-electron (3c/4e) interaction in an MO perspective. The strength of this

interaction (ΔE_s) scales with the inverse of the energy difference between the Te LP and the empty antibonding (σ_{BC}^*) states ($\Delta E_{n_A-\sigma_{BC}^*}$), while being proportional to their orbital overlap (Figure 3b). The strongest LP-delocalization-induced hyperbonding would then be expected when the relevant energy difference is small while the orbital overlap is maximized. A perfect hyperbonding situation may correspond to the case in which an LP of Te is completely delocalized over the relevant three atoms, resulting in the formation of two identical hyperbonds (Figure 3a-iii). However, it is also possible that an LP is delocalized only partially, with the formation of resultant short and long bonds. This situation is shown in Figure 3a-ii. In *a*-GST, a significant population of Te LPs are involved in such a weak interaction, intermediate between 2c/2e and 3c/4e interactions. The involvement of the antibonding states may be verified by the presence of occupied antibonding states near the top of the valence band for the hyperbonds (Figure 3c). In summary, by combining the hyperbonding concept with the conventional Lewis picture of bonding, one can now describe comprehensively all the local bonding of structural units (or all the chemical interactions) observed in *a*-GST.

4. Properties of PCMs from the Hyperbonding Perspective

With the help of the concept of multi-center hyperbonding, we can better understand various experimental and theoretical observations in *a*-GST, which have often been considered as being unusual.

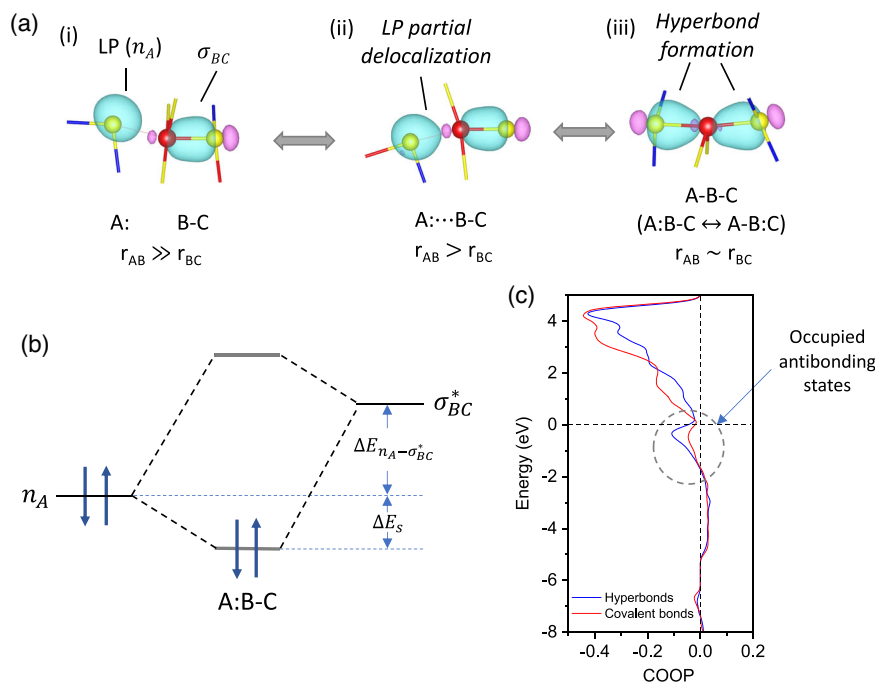


Figure 3. Hyperbonding mechanism. a) Sequential formation of hyperbonds through the gradual delocalization of an LP of an A atom to an antibonding orbital of an atom pair (B–C). Note the MLWF for the bond depicted is a bonding orbital rather than an antibonding one. b) A schematic energy diagram elucidating the energy-lowering process via the LP delocalization. c) Crystal orbital overlap population (COOP) curves for hyperbonds and ordinary covalent bonds of Sb(4,1) units in *a*-GST. The occupied antibonding states (negative COOP values) near the top of the valence band are highlighted.

4.1. Amorphous PCMs

4.1.1. Coordination Number

We first consider the impact of multi-center hyperbonding on the local coordination of atoms. The increased coordination number (CN) of constituent atoms beyond the octet rule in amorphous GST is a natural consequence of the multi-center nature of hyperbonding interactions. As stated before, the octet rule says that the maximum number of bonding and non-bonding electron pairs associated with an atom is four for the main-group elements with their four available AOs (one *s* and three *p* orbitals). However, this rule is no longer valid in GST, as shown in previous sections, and the sum of bonding and non-bonding electron pairs routinely exceeds four, with often (near-) octahedral coordination (CN \approx 5) being observed.^[9,26] In the hyperbonding picture, octahedral coordination is, in principle, feasible via three mutually perpendicular hyperbond pairs generated between three *p* AOs of a central atom and six AOs of six nearest ligand atoms. The strongest hyperbonding interaction is usually achieved when the involved AOs of the central and ligand atoms have a purely *p* character, because the maximum orbital overlap between the two *p* AOs is expected in this case. The coordination involving less than three hyperbond pairs corresponds to the seesaw (possessing a single pair of hyperbonds) or square-pyramidal (two perpendicular hyperbond pairs) molecular geometry, with a single non-bonding LP electron on the central atom. These local geometries are in accord with the VSEPR perspective. It is noted that such hyperbonding configurations are not rare in molecules: for example, SF₄, PF₅, or SF₆ exhibit seesaw, square-pyramidal, and octahedral molecular geometries, respectively.^[20,27] However, there exists an important difference between the molecules and *a*-GST. Unlike the molecules denoted, the coordination of some of the ligand Te atoms of hyperbond pairs in *a*-GST becomes differentiated as a result of one of their LPs being involved in hyperbonding. For instance, a Te(2,2) unit tends to form a hyperbond pair with a neighboring bonded atom pair, transforming to a Te(3,1) unit. A signature of hyperbonding, therefore, may be indicated by the abundance of threefold coordinated Te(3,1) units in chalcogenides.

4.1.2. Peierls Distortion

The phenomenon of a Peierls distortion in crystalline materials, which induces a periodic repetition of short and long bonds along particular crystallographic directions, has often been used to rationalize the presence in *a*-GST of a (near) linear triatomic bonding motif, consisting of a pair of short and long bonds.^[28] Such a structural correlation over three adjacent atoms appears to be generally found in *a*-PCMs, even in their liquid phases.^[29] The theory of the Peierls distortion for disordered systems is, however, quite uncertain. Instead, the long-and-short bonding motif found in amorphous or liquid PCMs can be simply considered as an outcome of weak hyperbonding interactions, as shown in Figure 3a-ii, in which the delocalization of an LP of an A atom is not complete enough to form two equal hyperbonds. It should be noted that, as Ge(3,1) or Sb(3,1) units in *a*-GST can be involved in such weak hyperbonding interactions with, in

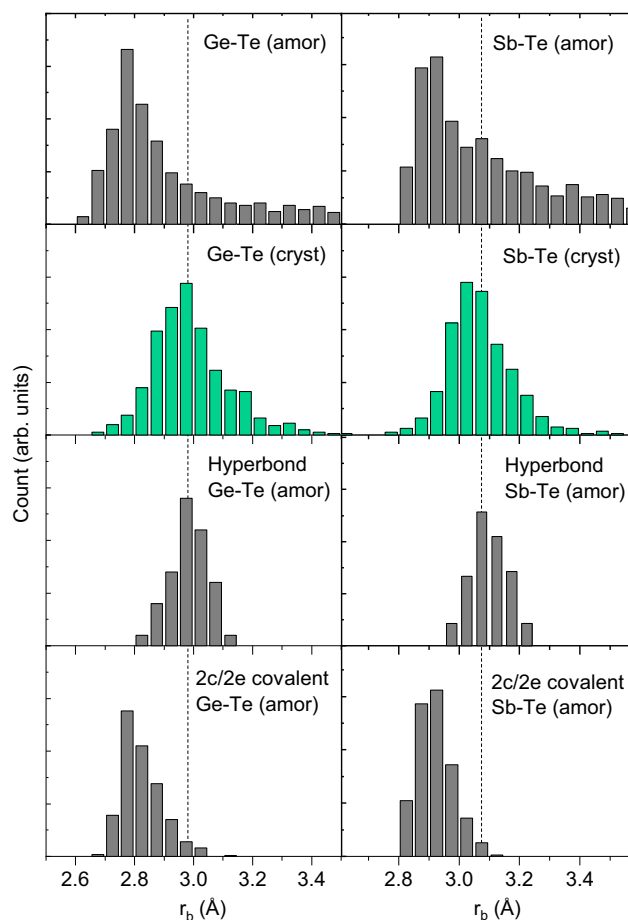


Figure 4. Distribution of interatomic distances found in *a*- and *c*-GST models. The interatomic distributions for all Ge–Te (left column) or Sb–Te (right column) pairs are decomposed into the corresponding contributions from hyperbonds (second panel from the bottom) and covalent bonds (bottom). These contributing sub-distributions are compared with the interatomic distances found in *c*-GST (second panel from the top).

principle, up to three neighboring Te LPs along three perpendicular axes, near-octahedral coordination is often recovered, once a sufficiently large interatomic distance (e.g., >3.5 Å) is used as a cutoff distance to define the first coordination shell. This result implies that weak hyperbonding interactions (Figure 3a-ii) play an important role in forming (although weakly connecting) the network structure of *a*-GST. As the extent of the LP-stabilization interaction with neighboring antibonding orbitals can vary considerably, depending on the distance between them, the interatomic distances for both short and long bonds are accordingly distributed widely (see the top panel in Figure 4). A broad distribution of interatomic distances could, thus, also be one of the indicators of active weak hyperbonding interactions, as found in *a*-GST.

4.1.3. Fast Crystallization

The smooth, continuous variation of interatomic distances resulting from hyperbonding interactions of varying strengths becomes interesting as soon as it is noticed that such a smooth distribution extends up to very long interatomic distances (≈ 4 Å),

much beyond the conventional upper bound of the nearest-neighbor bond distance of 3.2 \AA .^[3] This extended nature of nearest-neighbor bonding interactions is a characteristic feature of amorphous tellurides, such as PCMs. As already noted in the previous section, the broad distribution of interatomic distances originates from the wide variability of the degree of LP-antibonding interactions, which allows for a broad spectrum of bonding strengths and, consequently, of interatomic distances. The insight gained from this static chemical-bonding feature turns out to be also useful for understanding the dynamical behavior of *a*-GST, in particular, its fast crystallization behavior. The starting point is to link the wide variability of the LP-antibonding-interaction strengths to facile local-structural changes. We assume that, if there exist considerable energy barriers for the transitions between the configurations in Figure 3a, the distribution of interatomic distances for the ordinary covalent and hyperbonding interactions has to be separated to a certain extent. The lack of two distinguishable peaks in the interatomic-distance distributions for both Ge–Te and Sb–Te atom pairs is, hence, an indication that the transitions in Figure 3a involve insignificant energy barriers along the interaction path. With this reasonable assumption, we argue that such a characteristic feature of LP-antibonding-orbital interactions allows for a substantial amount of flexibility in local structural changes in *a*-GST at temperatures above its glass-transition temperature.^[9] As a result, the bond-switching transition between the configurations A: + B–C (in Figure 3a-i) and A–B + :C (the B–C bond now broken in Figure 3a-iii) is facilitated by the presence of the A–B–C hyperbond configuration with insignificant energy barriers.^[14] This LP-delocalization-assisted formation of hyperbonds, and bond switching, is exactly in line with reported facile valence-charge redistributions, which provides a route for the fast crystal nucleation-and-growth processes in *a*-GST,^[3,9] a characteristic feature of PCMs. In principle, the presence of weak hyperbonding interactions plays a crucial role in the bond-switching process, as its wide variability in interaction strength makes the facile switching process possible.

4.2. Crystalline PCMs

4.2.1. Structure of Crystalline GST

We have discussed so far how the hyperbonding concept can be linked to a variety of material properties of *a*-GST. Another important class of PCM (GST) material is its crystalline phase (*c*-GST). Two types of crystalline phases have been reported for GST: the metastable distorted-rock-salt phase, and the hexagonal phase stable at higher temperatures. We consider here only the former distorted-rock-salt phase, because this metastable phase is the only crystalline form actually involved in optical, or electronic, PC memory-device operations. In the ideal rock salt *c*-GST, tellurium atoms form an fcc sublattice, and Ge and Sb atoms occupy the other fcc sublattice, creating sixfold octahedral symmetries around all atomic species. Due to the vacancies occupying 20% of cationic sites in the composition GST, the average CN of Te becomes less than six, although the actual coordination for individual Te atoms depends on the local spatial distribution of the vacancies. A random distribution of cation vacancies over the available cation sites is commonly assumed, whose point of

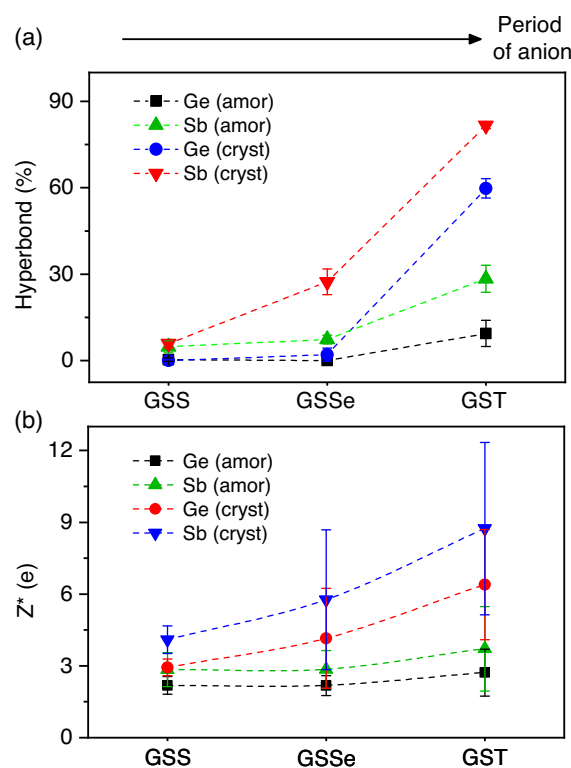


Figure 5. Correlation between the number of hyperbonds and BECs, Z^* . a) The percentages of Ge or Sb atoms (either in *a*- or *c*-GST) involved in hyperbonding are compared. b) The BECs corresponding to Ge or Sb atoms (either in *a*- or *c*-GST) are shown.

view is partially supported by experiments.^[11] Because of the presence of the vacant sites, the local coordination of each atom is distorted away from the perfect octahedral coordination, leading to overall a distorted-rock-salt structure. Despite this structural distortion, the crystalline symmetry still renders most of the Ge and Sb atoms to reside in near-octahedral ligand environments, allowing for a maximum three pairs of hyperbonds, each aligning along one of the three axes of an octahedron. This is not the case for *a*-GST, where a large proportion of the cations are surrounded by fewer than six ligand atoms. This means that the conditions necessary for hyperbond formation, i.e., a (near-) linear alignment of AOs, are intrinsically satisfied in *c*-GST, whereas this is not the case for *a*-GST. Naturally, the ratio of hyperbonds to ordinary covalent bonds in *c*-GST is much higher than that for *a*-GST (Figure 5a). We can link this observation to various property contrasts between *c*- and *a*-GST. Before doing so, however, we would like to establish the similarities and differences in the nature of chemical-bonding interactions between the amorphous and crystalline phases.

4.2.2. The Nature of Chemical Bonding in *c*-GST

Figure 6 shows the chemical-bonding indicators of the electron-localization function (ELF_b) and charge density (ρ_b) at bond (b) critical points evaluated for interatomic distances up to 4.0 \AA in *c*-GST, overlapped with the data for *a*-GST. The distributions of interatomic distances for ordinary covalent bonds and

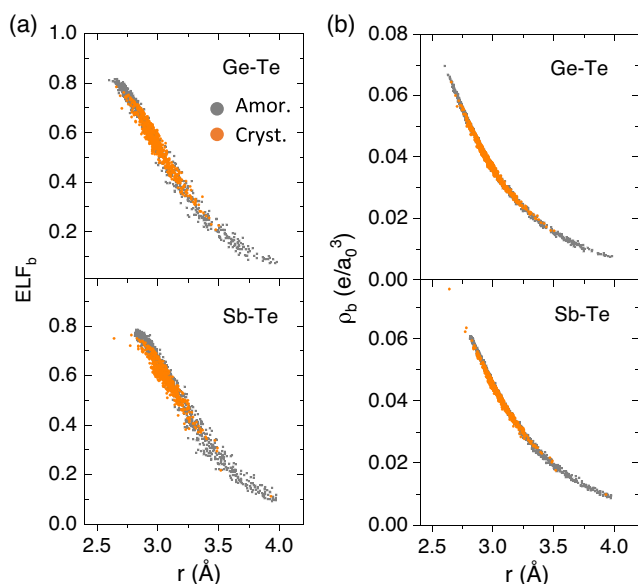


Figure 6. Chemical-bonding indicators for Ge–Te or Sb–Te pairs in GST as a function of their interatomic distances. a) The distributions of ELF_b at bond critical points for *a*- and *c*-GST are overlaid. b) The corresponding charge densities at the bond critical points are also shown.

multi-center hyperbonds in *a*-GST are also shown in Figure 4, wherein the overall distribution of interatomic distances for *a*-GST is well divided into two separate sub-peaks. It becomes clear from the similarity in the peak position and the distribution of interatomic-distance data that the bond-length distribution of *c*-GST closely resembles that of the hyperbonds in *a*-GST. Also, the corresponding chemical-bonding indicators for *c*-GST are nicely overlapped over the whole interatomic distances considered. These two observations strongly indicate that the nature of chemical-bonding interactions in *c*-GST is very similar to that of the subgroup of bonding interactions at the same distances in *a*-GST, namely, consisting of hyperbonds, such that there is a one-to-one correspondence between them in the plot in Figure 6. The additional tails in *a*-GST at shorter interatomic distances (less than ≈ 2.8 Å) and at longer interatomic distances (greater than ≈ 3.2 Å) correspond to ordinary covalent interactions (similar to B–C in Figure 3a-i) and the interatomic interactions caused by weak hyperbonding interactions (similar to A···B in Figure 3a-ii), respectively. Therefore, the classification developed for the chemical interactions in *a*-GST can be similarly adopted for describing the crystalline GST system. In this scheme, the overall structure of *c*-GST can be approximately described by a hyperbonding-prevalent network structure, whereas the chemical interaction in *a*-GST is instead dominated by ordinary covalent bonds with a minor population of weak/strong hyperbonding interactions. This difference leads to an unusual contrast in a diversity of material properties, which will be discussed in the following section.

4.3. Comparison Between *a*- and *c*-GST

We now return to the initial question, raised at the beginning of this article, of why there should exist a significant difference

in optical/electronic properties between *a*- and *c*-GST, although the implication from the fast crystallization capability of *a*-GST leads to quite the opposite conclusion. Also, the small difference in thermal conductivity between *a*- and *c*-GST is unusual, compared with, for instance, sp^3 -bonded semiconductors. This problem can be approached by considering the similarities and differences in chemical bonding between both phases, in particular, by focusing on the role of multi-center hyperbonding interactions.

4.3.1. Anharmonicity of *c*-GST and Small Thermal-Conductivity Difference

Multi-center hyperbonding seemingly has a close relationship with the high phonon anharmonicity and consequent low thermal conductivity of *c*-GST. This is due to the recent observation that long-ranged interactions in cubic crystalline compounds, which cause optical phonon softening and a strong phonon anharmonicity and scattering, have a fundamental root in the cubic crystalline structure enabling a linear alignment of *p* AOs.^[12] Except for ionic compounds, therefore, any crystals that have similar crystalline symmetries allowing for (near-) linear local coordination have the potential to exhibit high anharmonicity with low thermal conductivities. Cubic or rhombohedral crystals with (near-) octahedral local coordination may be a representative example of this type of material. Indeed, chalcogenides with these structures, such as IV–VI or I–V–VI₂ compounds, do show unusually small thermal conductivities.^[30] The significance of the linearity of atomic alignments, a common requirement for long-ranged interactions in crystals and for linear triatomic *p*–*p*–*p* orbital alignments for hyperbonding, points to a close relationship between the active hyperbonding in crystals and the large anharmonicity of the crystal lattice. As amorphous materials, including *a*-GST, generally exhibit low thermal conductivities due to disorder-induced scattering of thermal phonons,^[31] this results in the small difference in thermal conductivity between *a*- and *c*-GST. On the other hand, this is not the case for semiconductor materials of sp^3 -bonded compounds, typical non-hyperbonding materials, which show a much larger contrast in thermal conductivities between their *a*- and *c*-phases. An argument based on a shallow double-well potential due to the weak Peierls distortion has also been given recently to explain the large anharmonicity of *c*-GST.^[11,28]

4.3.2. BEC and Optical Contrast

The observed much stronger tendency for hyperbonding in *c*-GST, compared with its amorphous counterpart, originates from its cubic crystalline symmetry that allows for near-linear alignments of AOs through near-octahedral coordination: with this linear geometry, the orbital overlap of the relevant three *p* AOs can be maximized, and the strongest degree of hyperbonding can be realized. Therefore, it is the near-cubic symmetry of *c*-GST, with near-octahedral coordination, that leads to an abnormally strong propensity toward hyperbonding. The large difference in hyperbonding tendency between amorphous and crystalline GST is reminiscent of the large optical contrast found between them. It is then a reasonable next step to find correlations, if any, between multi-center hyperbonding and dielectric properties.

As the dielectric properties are closely linked to the BECs of the atomic constituents,^[32] Lee and Elliott^[14] have studied the correlation with the BECs instead. The BECs for the elements in *c*-GST are, in general, much larger than those for its amorphous counterpart (Figure 5b), which follows the trend of hyperbond/covalent bond ratios (Figure 5a). This similarity may be indicative of a close correlation between a high BEC and a strong tendency of hyperbonding. To check the validity of this conjecture, the BEC data were classified into different groups, each group of atoms being involved in forming a specific number of hyperbond pairs. An intimate correlation was then revealed: Ge or Sb atoms associated with more hyperbond pairs show a higher mean BEC, clear evidence that multi-center hyperbonding tends to induce high BECs and, consequently, increases the dielectric constants of materials (Figure 7). In this respect, it is the structure of *c*-GST that enables the large optical contrast between *a*- and *c*-GST. This conclusion is further supported by the observation that most other known *c*-PCMs possess similar crystalline structures, such as distorted-rock-salt, or rhombohedral structures, the former corresponding to *c*-Ge–Sb–Te or *c*-Ag–In–Sb–Te alloys, and the latter to *c*-GeTe, for instance.

4.4. Comparison Between Phase-Change and Non-Phase-Change Chalcogenides

The relationship of hyperbonding with material properties of *a*- and *c*-GST, established in the previous sections, is here extended to address the associated question of why only certain types of chalcogenides (viz., tellurides) exhibit the properties appropriate for PC applications.

4.4.1. Hyperbonding Tendency

As noted previously, *sp*³-bonded compounds are the most representative non-hyperbonded materials, in which only 2*c*/2*e* covalent bonds are present. Among chalcogenides, many sulfides or selenides also belong to this group. In most cases, this class of

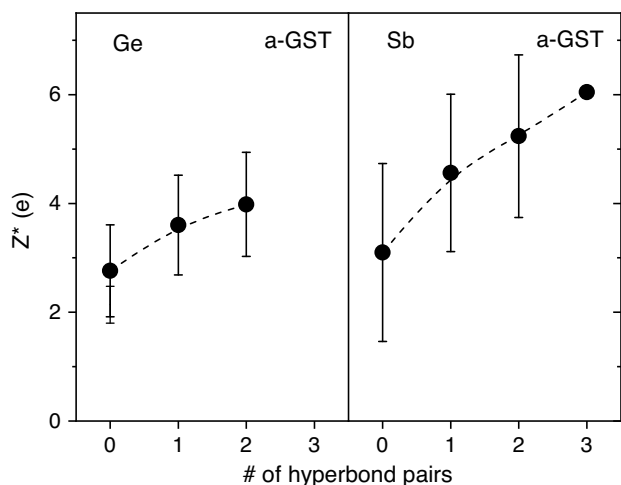


Figure 7. BECs (Z^*) of Ge or Sb atoms in *a*-GST as a function of their associated number of hyperbond pairs. For a given number of hyperbond pairs, Sb atoms always show a higher mean Z^* than Ge atoms.

materials shows none of the characteristic features of PCMs discussed so far, and therefore, these are non-PCMs. An interesting comparison among chalcogenides with different chalcogen species is presented in Figure 5a, from which the dependence of the hyperbonding tendency on chalcogen species can be directly deduced. In the case of amorphous phases, although a non-negligible percentage of hyperbonds is observed for both sulfide, $\text{Ge}_2\text{Sb}_2\text{S}_5$ (GSS) and selenide, $\text{Ge}_2\text{Sb}_2\text{Se}_5$ (GSSE) variants of GST, they show a much weaker hyperbonding tendency than *a*-GST. Figure 5a shows the percentage of hyperbonds, showing a clear trend of a small increase in the percentage of hyperbonds from *c*-GSS to *c*-GSSE, and then a steeper increase from *c*-GSSE to *c*-GST for both Ge and Sb central atoms. In comparison, the same trend is also observed in amorphous models, but their relative percentages are much lower than for the crystalline counterparts. Consequently, the difference between the amorphous and crystalline models drastically decreases from GST to GSS. This means that, although the hyperbond formation is indeed enhanced in all crystalline models in comparison with their amorphous counterparts, the amplification effect by adopting the cubic crystalline structure largely diminishes when Te is replaced by S or less significantly by Se. Hence, it can be concluded that, in terms of chalcogen types, the hyperbonding tendency sharply increases down the group-VI column of the periodic table, such that 3*c*/4*e* hyperbonding interactions in GST are much more stable than in GSS or GSSE, although GSSE exhibits a slightly higher hyperbonding tendency than GSS. This behavior can be understood in terms of the trend in hyperbonding interaction energy, which is inversely related to the bandgap of the material: sulfides have larger bandgaps than selenides, and, in turn, larger than tellurides. Thus, only GST shows a huge enhancement of hyperbonding, when it adopts the cubic crystalline form.

4.4.2. Born Effective Charge

As shown in Figure 5b, the first noticeable observation is that, except for the constituents in *a*-GSS and *a*-GSSE, the averaged BECs show higher values than their nominal ionic charges. Also, BECs for crystals are, in general, larger than those for their amorphous counterparts. The overall trend of BEC variation with different types of chalcogen anions resembles that of hyperbonds: from GSS to GSSE to GST, a gradual increase in the average BEC is observed, together with an increase in the difference between *a*- and *c*-models, which is basically the same as the trends observed for hyperbonds. This finding then answers the question of why large optical contrasts are seldom observed in sulfides or selenides. As shown earlier, their crystalline structures do not support 3*c*/4*e* hyperbonding, and ordinary 2*c*/2*e* covalent bonding prevails for both amorphous and crystalline phases of these materials (Figure 5). The relationship between aligned *p* orbitals and dielectric constants was similarly discussed for other chalcogenides recently.^[33] Such a strong dependence of multi-center interactions on chalcogen types can be understood from the factors that underlie the physics of the LP-delocalization-induced stabilization and hyperbonding (Figure 3b). In particular, most tellurides have sufficiently small energy differences between LPs and antibonding levels (approximately represented by the bandgap) and large AO overlaps, favorable

for multi-center interactions. However, this is not the case for sulfides or selenides, with larger bandgaps and smaller AOs.

5. Chemical-Bonding Models

Several chemical bonding models have been proposed to understand the structure and properties of chalcogenides and PCMs. We briefly discuss some of such recently proposed models for comparison. The resonant-bonding model^[34] deals with valence electrons delocalized over the whole lattice; therefore, this model is basically suitable for crystalline materials or, at least, materials with very significant long-range structural and chemical order. This model provides conceptual ideas for understanding large CNs of constituent atoms, unusual dielectric properties, or the weak *sp* hybridization of AOs for *c*-PCMs in terms of unsaturated covalent bonds with a bond order smaller than one. Nevertheless, the limitation of this model lies in describing crystals involving significant structural disorder, such as *c*-GST. Also, as aforementioned, appreciable delocalization-induced resonance (i.e., hyperbonding) exists even in *a*-GST, with their bonding properties being equivalent to the bonds in *c*-GST. More recently, the metavalent-bonding model^[35] has been proposed, based on the 2D “map” of compounds constructed as the functions of the delocalization index (or bond order) and charge transfer (or ionicity) between bonded atoms. This map successfully separates materials with different bonding types, including the proposed “metavalent bonding,” coined to emphasize the intermediate nature between metallic and covalent bonding. A similar map was also presented based on the resonant-bonding model with similar variables of hybridization (or covalency) and ionicity.^[8]

In a sense, the concept of hyperbonding shares a common feature with the resonant- (or metavalent-) bonding perspective, as all the models involve delocalization of valence electrons participating in bonding beyond the 2*c*/2*e* covalent bonds. The advantage of the hyperbonding concept, however, is that the requirement of long-range structural order can be avoided in describing electron delocalization, as the extent of delocalization reaches only up to three atomic centers in this model. Because of this, this model can provide a theoretical basis for understanding both amorphous and crystalline semiconductors within the existing conventional bonding frameworks in chemistry, i.e., 2*c*/2*e* and 3*c*/4*e* bonding interactions, without invoking completely new interactions. More importantly, the hyperbonding model can provide a simple, yet practically very important, criterion as to the structural characteristic required of crystals to be suitable for PCM or thermoelectric-material design, viz., a (near-) linear alignment of AOs leading to substantial hyperbonding interactions. This structure–property relationship, proposed by the hyperbonding model, which is lacking in other models, can be tested in future, and used for selecting candidate materials, simply by considering their crystalline structures utilizing available crystallographic data.

Although we have focused here on PCMs consisting only of *p*-block elements, PCMs containing transition metals,^[36] as well as tellurium-free PCMs (such as Sb-containing alloys^[37]), have also been actively investigated. We believe that hyperbonding interactions can also occur in these materials too, and so it will be interesting to investigate this in future studies.

6. Conclusion

The need for a new chemical-bonding theory for PCMs beyond the Lewis two-center, two-electron (2*c*/2*e*) covalent-bond concept arises, in principle, due to the complicated local bonding configurations in amorphous (*a*-) PCMs. In particular, it is the (near-) linear triatomic bonding configuration found therein that is inexplicable within the conventional covalent-bonding picture. The three-center, four-electron (3*c*/4*e*) hyperbonding concept recently proposed by us provides a sound theoretical basis for comprehending this three-body bonding configuration. With the help of this model, the chemical interactions constituting *a*-GST can be comprehensively described in terms of 2*c*/2*e* ordinary covalent bonds and 3*c*/4*e* hyperbonds. This classification is found to be similarly applicable to crystalline (*c*-) GST, such that a diversity of interesting (or unusual with respect to non-PCM) material properties of GST can then be accounted for, based on the unique bonding characteristics of hyperbonds and their abundance in materials of interest. The material properties considered in this review include the tendency toward high CNs of constituent atoms, being incompatible with the 8-*N* or octet rule, abnormally large BECs, the large optical contrast between *a*- and *c*-GST, and even the dynamical property of the fast crystallization speed of *a*-GST. Another useful aspect of the multi-center hyperbonding model is that it provides a comprehensive tool for defining structural motifs in terms of the number of associated LPs, covalent bonds, and hyperbonds with the help of the VSEPR theory. This greatly simplifies the description of not only GST but also any PCMs involving complicated bonding configurations caused by the delocalization of valence electrons beyond 2*c*/2*e* interactions. The hyperbonding concept, therefore, provides a useful chemical-bonding framework for a diversity of main-group chalcogenides, including PCMs.

Acknowledgements

The authors acknowledge the financial support of the UK EPSRC grants (EP/N022009, EP/M015130). Computational resources were provided by the ARCHER UK National Supercomputing service (HEC Materials Chemistry Consortium), which was funded by EPSRC (EP/L000202, EP/R029431).

Conflict of Interest

The authors declare no conflict of interest.

Keywords

chalcogenides, chemical bonding, density-functional theory (DFT)-molecular dynamics, multi-center hyperbonding, phase-change materials

Received: November 5, 2020

Revised: December 22, 2020

Published online:

[1] a) G. N. Greaves, S. Sen, *Adv. Phys.* **2007**, *56*, 1; b) S. R. Elliott, *Nature* **1991**, *354*, 445; c) C. A. Angell, *Science* **1995**, *267*, 1924.

- [2] a) J. Akola, R. O. Jones, *Phys. Rev. B* **2007**, *76*, 235201; b) T. H. Lee, D. Loke, S. R. Elliott, *Adv. Mater.* **2015**, *27*, 5477.
- [3] T. H. Lee, S. R. Elliott, *Phys. Rev. Lett.* **2011**, *107*, 145702.
- [4] a) S. Curtarolo, G. L. W. Hart, M. B. Nardelli, N. Mingo, S. Sanvito, O. Levy, *Nat. Mater.* **2013**, *12*, 191; b) P. Zhang, Z. J. Wang, X. X. Wu, K. Yaji, Y. Ishida, Y. Kohama, G. Y. Dai, Y. Sun, C. Bareille, K. Kuroda, T. Kondo, K. Okazaki, K. Kindo, X. C. Wang, C. Q. Jin, J. P. Hu, R. Thomale, K. Sumida, S. L. Wu, K. Miyamoto, T. Okuda, H. Ding, G. D. Gu, T. Tamegai, T. Kawakami, M. Sato, S. Shin, *Nat. Phys.* **2019**, *15*, 41.
- [5] D. Loke, T. H. Lee, W. J. Wang, L. P. Shi, R. Zhao, Y. C. Yeo, T. C. Chong, S. R. Elliott, *Science* **2012**, *336*, 1566.
- [6] A. Jain, Y. Shin, K. A. Persson, *Nat. Rev. Mater.* **2016**, *1*, 13.
- [7] a) N. Yamada, E. Ohno, K. Nishiuchi, N. Akahira, M. Takao, *J. Appl. Phys.* **1991**, *69*, 2849; b) M. Wuttig, N. Yamada, *Nat. Mater.* **2007**, *6*, 824; c) H. S. P. Wong, S. Raoux, S. Kim, J. Liang, J. P. Reifenberg, B. Rajendran, M. Asheghi, K. E. Goodson, *Proc. IEEE* **2010**, *98*, 2201.
- [8] D. Lencer, M. Salinga, B. Grabowski, T. Hickel, J. Neugebauer, M. Wuttig, *Nat. Mater.* **2008**, *7*, 972.
- [9] T. H. Lee, S. R. Elliott, *Adv. Mater.* **2017**, *29*, 1700814.
- [10] a) J. Ma, O. Delaire, A. F. May, C. E. Carlton, M. A. McGuire, L. H. VanBebber, D. L. Abernathy, G. Ehlers, T. Hong, A. Huq, W. Tian, V. M. Keppens, Y. Shao-Horn, B. C. Sales, *Nat. Nanotechnol.* **2013**, *8*, 445; b) Z. Zheng, X. L. Su, R. G. Deng, C. Stoumpos, H. Y. Xie, W. Liu, Y. G. Yan, S. Q. Hao, C. Uher, C. Wolverton, M. G. Kanatzidis, X. F. Tang, *J. Am. Chem. Soc.* **2018**, *140*, 2673; c) Y. Yu, M. Cagnoni, O. Cojocaru-Miredin, M. Wuttig, *Adv. Funct. Mater.* **2020**, *30*, 1904862.
- [11] T. Matsunaga, N. Yamada, R. Kojima, S. Shamoto, M. Sato, H. Tanida, T. Uruga, S. Kohara, M. Takata, P. Zalden, G. Bruns, I. Sergueev, H. C. Wille, R. P. Hermann, M. Wuttig, *Adv. Funct. Mater.* **2011**, *21*, 2232.
- [12] S. Lee, K. Esfarjani, T. F. Luo, J. W. Zhou, Z. T. Tian, G. Chen, *Nat. Commun.* **2014**, *5*, 3525.
- [13] W. G. Zeier, A. Zevalkink, Z. M. Gibbs, G. Hautier, M. G. Kanatzidis, G. J. Snyder, *Angew. Chem. Int. Ed.* **2016**, *55*, 6826.
- [14] T. H. Lee, S. R. Elliott, *Adv. Mater.* **2020**, *32*, 2000340.
- [15] W. A. Harrison, *Electronic Structure and The Properties Of Solids: The Physics of The Chemical Bond*, Dover Publications, Mineola, NY, USA **1989**.
- [16] N. Marzari, A. A. Mostofi, J. R. Yates, I. Souza, D. Vanderbilt, *Rev. Mod. Phys.* **2012**, *84*, 57.
- [17] P. L. Silvestrelli, N. Marzari, D. Vanderbilt, M. Parrinello, *Solid State Commun.* **1998**, *107*, 7.
- [18] A. V. Kolobov, P. Fons, J. Tominaga, S. R. Ovshinsky, *Phys. Rev. B* **2013**, *87*, 165206.
- [19] F. Weinhold, C. R. Landis, *Valency and Bonding: A Natural Bond Orbital Donor–Acceptor Perspective*, Cambridge University Press, Cambridge, UK **2005**.
- [20] J. I. Musher, *Angew. Chem. Int. Ed.* **1969**, *8*, 54.
- [21] A. E. Reed, L. A. Curtiss, F. Weinhold, *Chem. Rev.* **1988**, *88*, 899.
- [22] R. J. Gillespie, R. S. Nyholm, *Q. Rev.* **1957**, *11*, 339.
- [23] G. C. Pimentel, *J. Chem. Phys.* **1951**, *19*, 446.
- [24] S. Shaik, D. Danovich, J. M. Galbraith, B. Braida, W. Wu, P. C. Hiberty, *Angew. Chem. Int. Ed.* **2020**, *59*, 984.
- [25] C. A. Coulson, *J. Chem. Soc.* **1964**, 1442.
- [26] A. Hirata, T. Ichitsubo, P. F. Guan, T. Fujita, M. W. Chen, *Phys. Rev. Lett.* **2018**, *120*, 205502.
- [27] M. C. Durrant, *Chem. Sci.* **2015**, *6*, 6614.
- [28] J.-P. Gaspard, *C. R. Phys.* **2016**, *17*, 389.
- [29] J. Y. Raty, V. Godlevsky, P. Ghosez, C. Bichara, J. P. Gaspard, J. R. Chelikowsky, *Phys. Rev. Lett.* **2000**, *85*, 1950.
- [30] a) D. T. Morelli, V. Jovovic, J. P. Heremans, *Phys. Rev. Lett.* **2008**, *101*, 4; b) Y. Z. Pei, H. Wang, G. J. Snyder, *Adv. Mater.* **2012**, *24*, 6125; c) M. D. Nielsen, V. Ozolins, J. P. Heremans, *Energy Environ. Sci.* **2013**, *6*, 570.
- [31] W. X. Zhou, Y. Cheng, K. Q. Chen, G. F. Xie, T. Wang, G. Zhang, *Adv. Funct. Mater.* **2020**, *30*, 1903829.
- [32] P. B. Littlewood, *Crit. Rev. Solid State Mater. Sci.* **1984**, *11*, 229.
- [33] B. Huang, J. Robertson, *Phys. Rev. B* **2010**, *81*, 081204.
- [34] a) G. Lucovsky, R. M. White, *Phys. Rev. B* **1973**, *8*, 660; b) K. Shportko, S. Kremers, M. Woda, D. Lencer, J. Robertson, M. Wuttig, *Nat. Mater.* **2008**, *7*, 653.
- [35] a) M. Wuttig, V. L. Deringer, X. Gonze, C. Bichara, J. Y. Raty, *Adv. Mater.* **2018**, *30*, 1803777; b) J. Y. Raty, M. Schumacher, P. Golub, V. L. Deringer, C. Gatti, M. Wuttig, *Adv. Mater.* **2019**, *31*, 1806280.
- [36] a) F. Rao, K. Y. Ding, Y. X. Zhou, Y. H. Zheng, M. J. Xia, S. L. Lv, Z. T. Song, S. L. Feng, I. Ronneberger, R. Mazzarello, W. Zhang, E. Ma, *Science* **2017**, *358*, 1423; b) J. M. Skelton, S. R. Elliott, *J. Phys.: Condens. Matter* **2013**, *25*, 205801.
- [37] a) S. Raoux, A. K. Koenig, H.-Y. Cheng, D. Garbin, R. W. Cheek, J. L. Jordan-Sweet, M. Wuttig, *Phys. Status Solidi B* **2012**, *249*, 1999; b) S. Raoux, C. Cabral, L. Krusin-Elbaum, J. L. Jordan-Sweet, K. Virwani, M. Hitzbleck, M. Salinga, A. Madan, T. L. Pinto, *J. Appl. Phys.* **2009**, *105*, 064918.



Tae-Hoon Lee earned his Ph.D. degree from POSTECH. He is currently a senior research associate with the Department of Engineering at the University of Cambridge. His current research focuses on the first-principles simulation of novel nanoparticles and amorphous/crystalline functional materials for various applications.



Stephen Elliott obtained his undergraduate and Ph.D. degrees from the University of Cambridge. He was a professor of chemical physics with the Department of Chemistry at Cambridge until 2019. He is currently an emeritus professor at Cambridge, a life fellow of Trinity College, Cambridge, and a visiting professor at the Universities of Oxford, Southampton, and Beihang (Beijing). His current research interests include the computer simulation of functional materials, such as phase-change-memory materials, using density-functional methods and machine-learned interatomic potentials.